

Optimized Diamond Quantum Photonics

Constantin Dory, Dries Vercruyse,[§] Ki Youl Yang,[§] Neil V. Sapra,
Alison E. Rugar, Shuo Sun, Daniil M. Lukin, Alexander Y. Piggott,
Jingyuan L. Zhang, Marina Radulaski,^{*} Konstantinos G. Lagoudakis,[†]
Logan Su and Jelena Vučković[‡]

E. L. Ginzton Laboratory, Stanford University, Stanford, California 94305, USA

[‡]Corresponding Author. E-mail: jela@stanford.edu

[§]These authors contributed equally.

May 29, 2022

Diamond photonics enables applications ranging from nonlinear optics, to quantum technologies, including quantum computing, networking and sensing. However, challenges in design and fabrication limit the geometry of diamond nanostructures and ultimately impede diamond photonics from evolving into a scalable, efficient platform. Recently developed inverse design methods in photonics utilize machine learning and optimization techniques to overcome difficult design problems, providing a superior method over traditional design approaches. In this report, we combine inverse design with a scalable fabrication technique to develop an optimized diamond quantum nanophotonic plat-

^{*}Also at: Electrical and Computer Engineering, University of California, Davis, CA 95616, USA

[†]Now at: Department of Physics, University of Strathclyde, Glasgow, G4 0NG, UK

form. We utilize the flexibility of inverse design to demonstrate a variety of fabrication-tolerant and efficient components necessary to enable scalable optical circuits at the single-photon level.

One Sentence Summary (125 characters): Inverse design enables a scalable diamond photonic platform.

Diamond has excellent material properties for quantum optics (1, 2), optomechanics (3, 4), or nonlinear optics (5). Of particular interest is the variety of color centers that diamond hosts, some of which exhibit very long coherence times (1, 6). The development of diamond photonic circuits (7) has therefore emerged as a promising route for implementing optical quantum networks (8–13), quantum computers (14–16) and quantum sensors (17). However, current diamond photonic devices are inefficient and have strongly constrained geometries and functionalities, impeding progress in the field, in particular for quantum technologies, which require operation at the level of single or few photons.

In this work, we overcome design and fabrication challenges in diamond and demonstrate an efficient, scalable diamond photonic platform. To this end, we employ inverse design methods, which have recently attracted considerable attention for their efficient design of nanophotonic devices with superior performance over conventional designs (18). This optimization technique allows a search through the full parameter space of fabricable devices, thereby leading to superior structures relative to conventional designs in efficiency, footprint, and functionality (19). To realize inverse-designed structures in diamond we employ a fabrication technique based on quasi-isotropic etching (20–22) with minimal fabrication constraints. Moreover, we can overcome remaining fabrication limitations by incorporating them as part of the inverse design optimization (23, 24).

Inverse Design of Diamond Nanophotonic Devices

As an example for a design challenge, we choose free-space optical interfaces, where state-of-

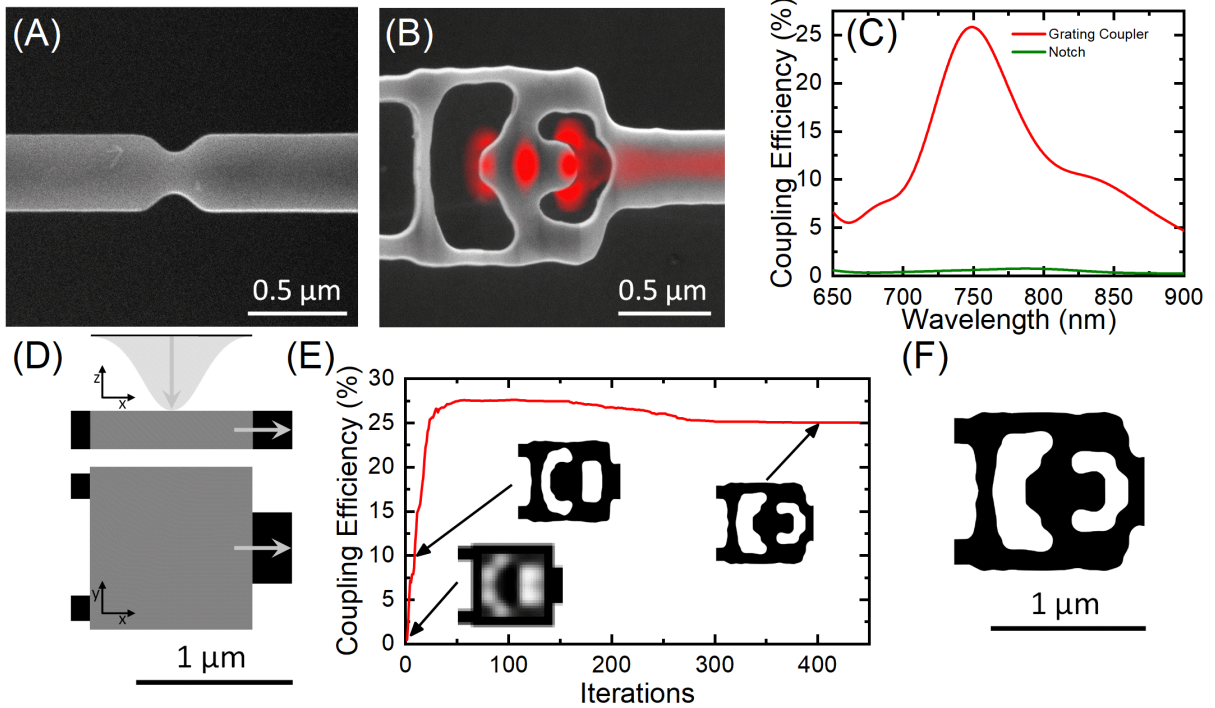


Figure 1: Inverse design of efficient nanophotonic interfaces. Scanning electron micrograph of (A) a notch and (B) an inverse-designed vertical coupler with simulated fields superimposed in red ($1.0 \times 1.0 \mu\text{m}^2$ footprint). (C) Simulated performance of the vertical coupler (red) and the notch (green). (D) Design set-up, where the gray area indicates the design area. (E) In-coupling efficiency during design optimization; insets illustrate different optimization phases. The small performance drop beyond 200 iterations of optimization is due to imposing fabrication constraints. (F) Final device structure after optimization.

the-art devices are notches (Fig. 1A) with only $\approx 1\%$ efficiency (15). This accumulates to a loss of $\approx 99.99\%$ in transmission experiments, which employ both in- and out-coupling between diamond photonic structures and free-space, and is indicative of the loss at any optically interfaced node in a quantum network. To improve on this, we develop an inverse-designed vertical coupler (Fig. 1B) that significantly outperforms the notch interface. The couplers have

a footprint of $1.0 \times 1.0 \mu\text{m}^2$ and couple directly to a 400 nm wide waveguide without the need of a tapering section, assuring compactness. As shown in Fig. 1C the simulated efficiencies of the coupler (red) and the notch (green) are $\approx 25\%$ and $\approx 1\%$ (15), respectively. The simulated structures are symmetric along the z-axis and as such have a theoretical maximum coupling efficiency of 50 %.

Inverse design problems in photonics are defined by an electromagnetic simulation, a design region and a figure of merit to optimize. The starting conditions of the simulation for vertical couplers are shown in Fig. 1D. A vertically incident Gaussian beam forms the source of the simulation and is centered above the $1.0 \times 1.0 \mu\text{m}^2$ design region shown in gray. To the left of the design region are two black support bars to suspend the design, and to the right is a black output waveguide. The light coupled into the fundamental TE mode of the waveguide serves as the figure of merit and is maximized during our optimization process (detailed in (25)). The coupling efficiency during the optimization is shown in Fig. 1E. At the start of the optimization, any permittivity value between that of air and diamond is allowed, which results in a continuous structure shown in the leftmost inset. After several iterations this structure is discretized, in which case the permittivity is that of either air or diamond. This discrete structure is further optimized while also gradually imposing a penalty on the fabricability. As a result, the coupling efficiency at a wavelength of 737 nm (silicon-vacancy color center zero-phonon line) peaks at a value of $\approx 27.5\%$, which then decreases to $\approx 25\%$ to comply with fabrication constraints (24).

Characterization of Diamond Vertical Couplers

To characterize the coupling efficiency of the vertical couplers, we measure the device shown in the scanning electron micrographs (SEM) in Figs. 2A and B, in top-down and side view, respectively. An optical microscope image of the same structure is presented in Fig. 2C, qualitatively showing the high performance of the vertical couplers. When a laser is coupled into the

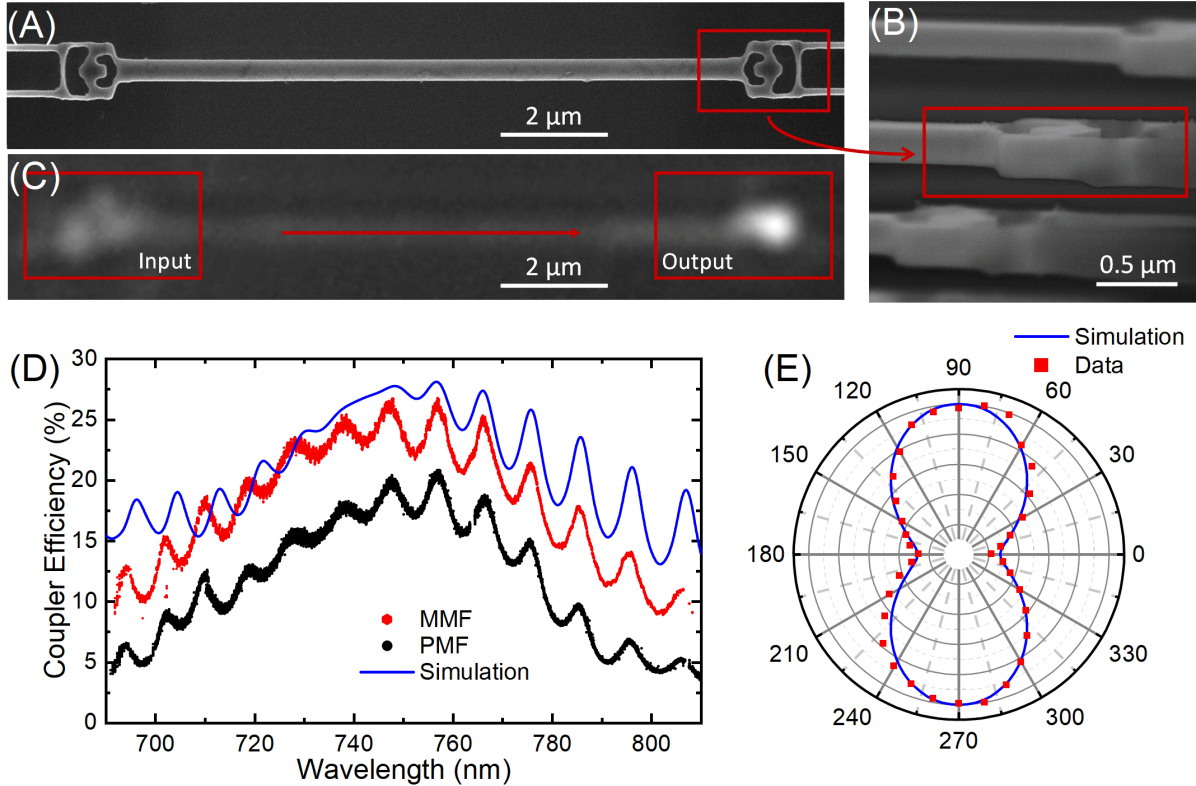


Figure 2: Inverse-designed vertical couplers. (A) Scanning electron micrograph of two vertical couplers connected by a waveguide, which are used to characterize the efficiency of the vertical couplers. (B) Sideview of the vertical coupler, showing the undercut of the structure at a 85° angle. (C) Optical microscope image when focusing a Gaussian beam on the coupler on the left (Input) and detecting the transmitted light from the coupler on the right (Output). (D) Characterization of the efficiency of a single vertical coupler, peak efficiencies exceed 20 % for single-mode polarization-maintaining fibers (PMF, black) and 26 % for multimode fibers (MMF, red). Numerical simulation results are shown as blue line. (E) Polarization scan shows that the vertical couplers preferentially couple to a Gaussian beam with a polarization perpendicular to the nanobeam, simulated polarization dependence shown as a blue line are in good agreement with the measured data (red squares).

left vertical coupler (Input), the output on the right vertical coupler (Output) is clearly visible, indicating the high coupling efficiency of the vertical couplers. For notches, the back-reflection at the input overpowers the outputted light by several orders of magnitude. The results of our efficiency measurements are presented in Fig. 2D. To quantitatively measure the efficiency, we use a continuous-wave tunable Ti:Sapphire laser, which we couple to the structures in a cryostat using a 0.9 NA objective. We then couple the resulting output beam to a single-mode polarization-maintaining fiber (PMF, black data points) and a multimode fiber (MMF, red data points). The experimental results show peak efficiencies of $> 20\%$ for PMF and $> 26\%$ for MMF, with broadband performance of $> 70\text{ nm}$ (PMF) and $> 90\text{ nm}$ (MMF). Moreover, the overall trend matches well with the numerically simulated efficiencies (blue line). The small discrepancy between the measurements with PMF and MMF suggests that we couple very efficiently from the waveguide mode back into the fundamental free-space mode. For data on the fabrication yield of the vertical couplers, we refer the reader to the supplementary materials of our work, where we analyze the transmission spectrum of 15 devices and find excellent overlap (see Fig. S4 in (22)). We further characterize the polarization dependence of the vertical couplers by sweeping the polarization of the input laser beam (red data points in Fig. 2E). We observe a five-fold reduction of the power measured in the detection fiber when rotating the polarization by 90° , which corresponds well to our simulated results (blue line in Fig. 2E).

In photonics, grating couplers are frequently used as efficient interfaces (26–31). Such designs typically use asymmetry along the z-axis, e.g. through partial etches (26, 27, 31) or material stacks with varying refractive indices (27) to achieve high coupling efficiencies. In diamond quantum photonics many of these approaches cannot be employed as current thin-film diamond on silica substrate platforms (28–30) do not support state-of-the-art quantum optics experiments (15, 16, 32). Similar approaches with hybrid structures, such as gallium phosphide (GaP) membranes on diamond, offer a platform for efficient grating couplers (33). However, the

optical field is confined in the GaP membrane and emitters only couple evanescently to the resonators. Symmetric vertical couplers for efficient out-coupling from suspended membranes into high NA objective have been demonstrated in the past (34), but the incoupling of this structure is highly inefficient. In contrast to the approaches mentioned above, our vertical couplers offer an interface that fulfills the requirements for integrated diamond quantum photonics: The vertical couplers are designed for suspended membranes, couple light in and out with high efficiencies and broadband performance, and are compact, as they do not require tapers. Furthermore, the design does not require any additional fabrication steps, has excellent fabrication yield and is robust to typical fabrication errors and misalignment (see Fig. S4 in (22)). Thus, vertical couplers represent an excellent example of the significance of inverse design in the development of photonic components. Ultimately, the implementation of scalable quantum networks requires efficiencies of building blocks close to unity. Efficiencies of $> 90\%$ can be achieved with fiber tapers (35), which is neither a compact nor scalable a solution. Our current design offers the advantage of compactness (1.0 μm vs. hundreds of μm), robust alignment (see Fig. S4 in (22)) and practicality in fabrication and measurements. Building on our work, similar efficiencies as fiber tapers may be within reach when increasing the fabrication complexity and adding partial etches or materials with different refractive indices to the design parameters (19).

Diamond Quantum Optical Interfaces

In the preceding section we demonstrated efficient coupling to rectangular waveguide modes. Now we investigate coupling to the modes of nanophotonic resonators, which are used in quantum optics to enhance the light-matter interaction (36) and facilitate efficient integration of quantum emitters into optical circuits. The studied devices, nanobeam photonic crystal (PhC) cavities host a TE mode and are shown in Fig. 3A and B. We center a supercontinuum light source on the left coupler, where the Gaussian beam couples to the TE fundamental mode in the nanobeam and subsequently into PhC modes. On the other end of the PhC, the light couples

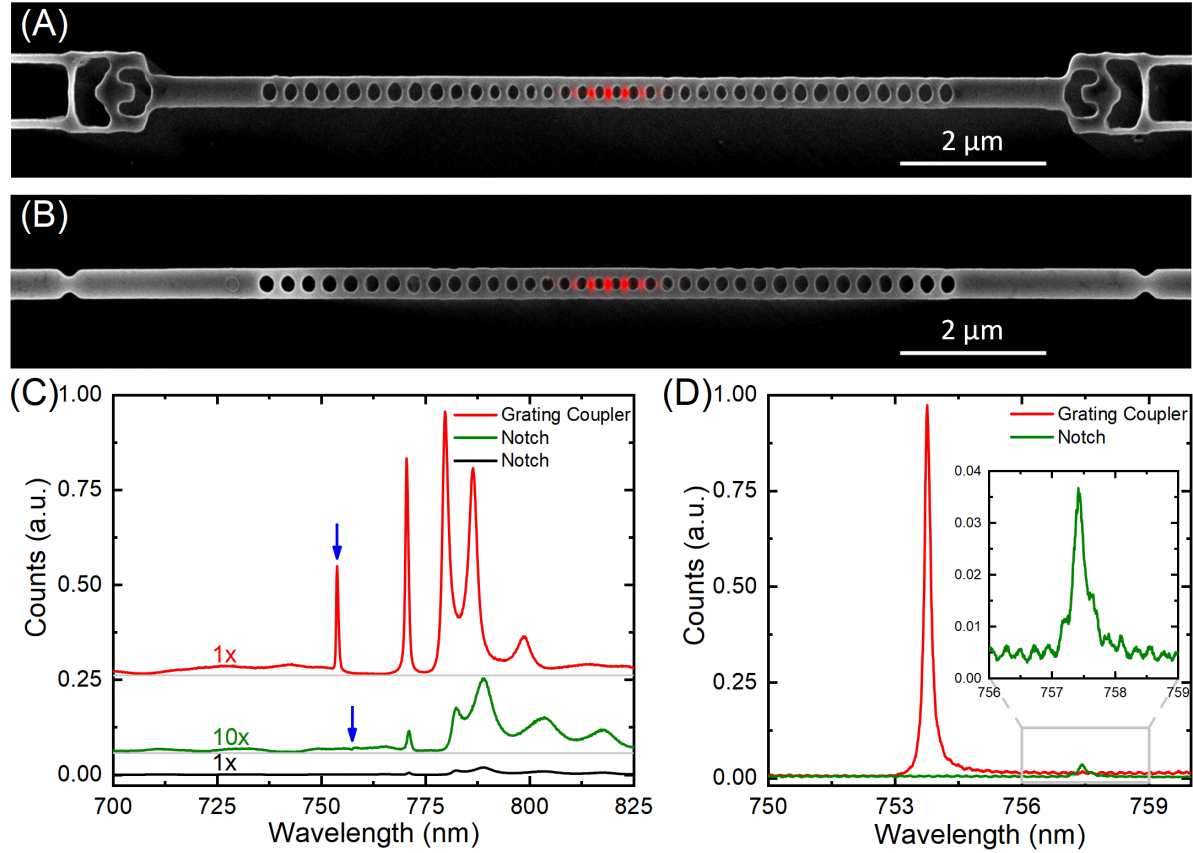


Figure 3: Suspended rectangular diamond nanobeams with optical interfaces. Scanning electron micrographs of nanobeam photonic crystal cavities in (A) with inverse-designed vertical couplers and in (B) with notches as interface for in- and out-coupling. Fields inside the cavities are depicted in red. (C) Transmission measurements using a supercontinuum light source, red spectrum corresponds to the coupler device in (A), black and green spectra to the notch device in (B). The spectra are offset for better visualization and the cavity resonances are indicated by blue arrows. (D) Spectra acquired by coupling supercontinuum light source directly to the cavity and out through a vertical coupler (red line) or a notch (green line). Inset corresponds to the data inside the gray box.

back into the TE fundamental mode of the nanobeam and through the coupler into the free-space fundamental mode. In Fig. 3C we present several stacked spectra measured using the method described above. The data in red correspond to the device with vertical couplers, while the black spectrum corresponds to a cavity with notches, using the same power and integration time. The count rates of the device with notches as an interface are more than two orders of magnitude smaller, for which we compensate by integrating 10 times longer and plot the spectrum in green. When comparing the cavity resonances (blue arrows), we find a > 550 -fold increase in counts of the vertical coupler over the notch device for comparable quality factors (≈ 4000). This result is comparable to the 625-fold enhancement that we expect from simulations and is equivalent to the expected increase in communication rates in quantum networks. This improvement in coupling efficiencies results in a dramatic decrease in experimental times – from weeks to minutes, thereby opening opportunities for larger scale experiments. In Fig. 3D we present spectra, where we couple the laser light directly to the cavity and optimize the alignment to collect maximum counts from the vertical coupler (red line) and the notch (green line). From this measurement we can conclude that the extraction efficiency of a vertical coupler is > 26 times greater than that of a notch.

Toward Diamond Photonic Circuits

For applications in quantum technologies, many nodes need to be connected to scale from single qubits to large, interconnected qubit arrays. However, up until now Y-splitters have posed a major challenge in suspended diamond photonics, as state-of-the-art fabrication using angled etch is not conducive to variations in the device geometry. In contrast, as shown in Fig. 4A, we can fabricate a circuit comprised of three components with completely different geometries: vertical coupler, beamsplitter, and nanobeam PhC cavity. The device is designed to interfere the transmission of two nanobeam PhC cavities at an inverse-designed Y-splitter with 50 : 50 splitting ratio and simulated efficiencies of 95 %. We address the cavities separately or simulta-

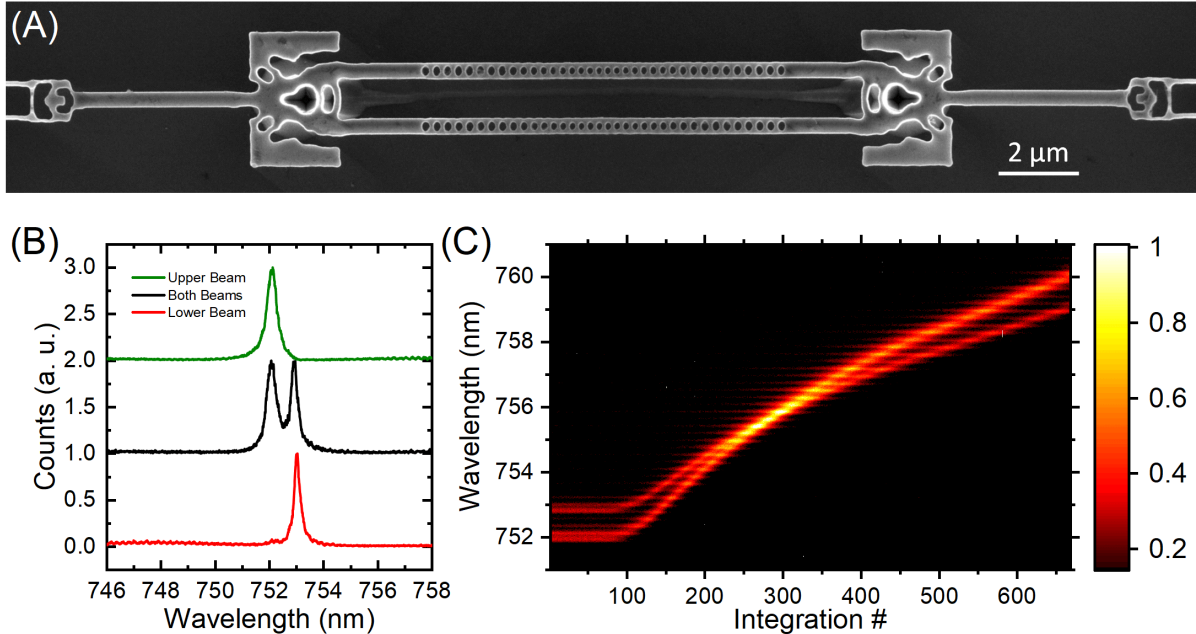


Figure 4: Toward diamond quantum nanophotonic circuits. (A) Scanning electron micrograph of a nanophotonic circuit, which interferes the signal from two nanophotonic devices and couples the signal off the chip. (B) Spectra of the nanobeams from the device shown in (A). Green, black and red data correspond to the upper, both and the lower nanobeam, respectively. (C) Demonstration that cavities with fabrication induced frequency offset can be tuned in resonance by gas tuning; colorbar corresponds to normalized counts.

neously by top-down excitation with a supercontinuum source focused on the cavities directly, as presented in Fig. 4B. The resonances of the two beams are detuned by < 1 nm because of fabrication imperfections. We overcome this detuning with a gas condensation method, as shown in Fig. 4C, where we tune two cavities into and out of resonance. Comparing the amplitudes of the cavity on and off resonance suggests constructive interference, indicating that the cavities are approximately in phase and have the same polarization. The simple proof-of-concept diamond photonic circuit presented in Fig. 4 could be achieved with classical photonics design. In

the broader context of diamond-based quantum information efforts, however, inverse-designed structures are advantageous to their traditional counterparts. Imperfect positioning of emitters, nonunity conversion efficiency of implanted ions to color centers, inhomogeneous broadening, and high material costs necessitate highly flexible and robust circuit design. Utilizing inverse design, we can overcome such limitations by designing compact circuits for arbitrary emitter locations and can assure phase-matching across different paths of the circuits as well as optimization for specific bandwidths (see (22) for details). Furthermore, utilizing inverse design devices such as vertical couplers and Y-splitters can be combined to increases compactness (25).

In summary, we realize a scalable, efficient diamond nanophotonic architecture (37) using the powerful combination of inverse design optimization and quasi-isotropic etching techniques. The quasi-isotropic etch enables the fabrication of a wide variety of device geometries, allowing us to utilize inverse-designed components to outperform traditionally designed diamond photonics. This progress lays the foundation for scaling to larger quantum networks (8, 10) with spins (6) embedded in quantum nodes. Furthermore, inverse design opens up a whole library of device components, including pulse shapers and splitter trees to drive quantum systems, phase delays, mode converters and optimized waveguides and cavities. In addition to diamond, inverse design can also be utilized to rapidly develop photonic circuits for promising material platforms that host quantum emitters and have challenging fabrication protocols, such as silicon carbide (38) and yttrium orthovanadate (39).

Acknowledgments: We acknowledge the help of Usha Raghuram and Elmer Enriquez with RIE. **Funding:** This work is financially supported by Army Research Office (ARO) (award no. W911NF1310309), Air Force Office of Scientific Research (AFOSR) MURI Center for Attojoule Nano-Optoelectronics (award no. FA9550-17-1-0002), Gordon and Betty Moore Foundation; C.D. acknowledges support from the Andreas Bechtolsheim Stanford Graduate Fellowship. K.Y.Y. and M.R. acknowledge support from the Nano- and Quantum Science and

Engineering Postdoctoral Fellowship. D.M.L. acknowledges support from the Fong Stanford Graduate Fellowship and the National Defense Science and Engineering Graduate Fellowship. D.V. acknowledges funding from FWO and European Unions Horizon 2020 research and innovation program under the Marie Skłodowska-Curie grant agreement No 665501. We thank Google for providing computational resources on the Google Cloud Platform. Part of this work was performed at the Stanford Nanofabrication Facility (SNF) and the Stanford Nano Shared Facilities (SNSF), supported by the National Science Foundation under award ECCS-1542152.

Author contributions: C.D. and J.V. conceived and designed the experiment. C.D. developed the fabrication, fabricated the sample and measured and analyzed the data. D.V., N.V.S., L.S. and C.D. conducted inverse design optimization of photonic components. K.Y.Y., D.M.L. and A.Y.P. contributed to the sample fabrication. A.E.R. and S.S. contributed to optical measurements. J.L.Z., M.R. and K.G.L. provided expertise. J.V. supervised the project. All authors participated in the discussion, understanding of the results, and the preparation of the manuscript.

Competing interests: The authors declare they have no competing financial interests. **Data and materials availability:** All data are available in the manuscript or the supplementary materials.

References

1. M. Atatüre, D. Englund, N. Vamivakas, S. Y. Lee, and J. Wrachtrup. Material platforms for spin-based photonic quantum technologies. *Nat. Mater.* **3**, 38–51 (2018).
2. D. D. Awschalom, R. Hanson, J. Wrachtrup, and B. B. Zhou. Quantum technologies with optically interfaced solid-state spins. *Nat. Photonics* **12**, 516–527 (2018).
3. B. Khanaliloo, H. Jayakumar, A. C. Hryciw, D. P. Lake, H. Kaviani, and P. E. Barclay. Single-crystal diamond nanobeam waveguide optomechanics. *Phys. Rev. X* **5**, 1–21 (2015).
4. M. J. Burek, J. D. Cohen, S. M. Meenehan, N. El-Sawah, C. Chia, T. Ruelle, S. Meesala, J. Rochman, H. A. Atikian, M. Markham, D. J. Twitchen, M. D. Lukin, O. Painter, and M. Lončar. Diamond optomechanical crystals. *Optica* **3**, 1404–1411 (2015).
5. B. J. M. Hausmann, I. Bulu, V. Venkataraman, P. Deotare, and M. Loncar. Diamond nonlinear photonics. *Nat. Photonics* **8**, 369–374 (2014).
6. B. C. Rose, D. Huang, Z. H. Zhang, P. Stevenson, A. M. Tyryshkin, S. Sangtawesin, S. Srinivasan, L. Loudin, M. L. Markham, A. M. Edmonds, D. J. Twitchen, S. A. Lyon, and N. P. De Leon. Observation of an environmentally insensitive solid-state spin defect in diamond. *Science* **361**, 60–63 (2018).
7. I. Aharonovich, A. D. Greentree, and S. Prawer. Diamond photonics. *Nat. Photonics* **5**, 397–405 (2011).
8. J. I. Cirac, P. Zoller, H. J. Kimble, and H. Mabuchi. Quantum state transfer and entanglement distribution among distant nodes in a quantum network. *Phys. Rev. Lett.* **78**, 3221 (1997).

9. H.-J. Briegel, W. Dür, J. I. Cirac, and P. Zoller. Quantum repeaters: The role of imperfect local operations in quantum communication. *Phys. Rev. Lett.* **81**, 5932 (1998).
10. H. J. Kimble. The quantum internet. *Nature* **453**, 1023–1030 (2008).
11. B. Hensen, H. Bernien, A. E. Dreaú, A. Reiserer, N. Kalb, M. S. Blok, J. Ruitenberg, R. F. Vermeulen, R. N. Schouten, C. Abellán, W. Amaya, V. Pruneri, M. W. Mitchell, M. Markham, D. J. Twitchen, D. Elkouss, S. Wehner, T. H. Taminiau, and R. Hanson. Loophole-free Bell inequality violation using electron spins separated by 1.3 kilometres. *Nature* **526**, 682–686 (2015).
12. S. Sun, J. L. Zhang, K. A. Fischer, M. J. Burek, C. Dory, K. G. Lagoudakis, Y.-K. Tzeng, M. Radulaski, Y. Kelaita, A. Safavi-Naeini, Z.-X. Shen, N. A. Melosh, S. Chu, M. Lončar, and J. Vučković. Cavity-enhanced Raman emission from a single color center in a solid. *Phys. Rev. Lett.* **121**, 083601 (2018).
13. M. A. Lemonde, S. Meesala, A. Sipahigil, M. J. Schuetz, M. D. Lukin, M. Loncar, and P. Rabl. Phonon networks with silicon-vacancy centers in diamond waveguides. *Phys. Rev. Lett.* **120**, 213603 (2018).
14. T. D. Ladd, F. Jelezko, R. Laflamme, Y. Nakamura, C. Monroe, and J. L. O’Brien. Quantum computers. *Nature* **464**, 45–53 (2010).
15. A. Sipahigil, R. E. Evans, D. D. Sukachev, M. J. Burek, J. Borregaard, M. K. Bhaskar, C. T. Nguyen, J. L. Pacheco, H. A. Atikian, C. Meuwly, R. M. Camacho, F. Jelezko, E. Bielejec, H. Park, M. Lončar, and M. D. Lukin. An integrated diamond nanophotonics platform for quantum-optical networks. *Science* **354**, 847–850 (2016).
16. R. E. Evans, M. K. Bhaskar, D. D. Sukachev, C. T. Nguyen, A. Sipahigil, M. J. Burek, B. Machielse, G. H. Zhang, A. S. Zibrov, E. Bielejec, H. Park, M. Lončar, and M. D.

Lukin. Photon-mediated interactions between quantum emitters in a diamond nanocavity. *Science* (2018).

17. C. L. Degen, F. Reinhard, and P. Cappellaro. Quantum sensing. *Rev. Mod. Phys.* **89**, 035002 (2017).
18. S. Molesky, Z. Lin, A. Y. Piggott, W. Jin, J. Vuckovic, and A. W. Rodriguez. Inverse design in nanophotonics. *Nat. Photonics* **12**, 659–670 (2018).
19. L. Su, A. Y. Piggott, N. V. Sapra, J. Petykiewicz, and J. Vučković. Inverse design and demonstration of a compact on-chip narrowband three-channel wavelength demultiplexer. *ACS Photonics* **5**, 301–305 (2018).
20. B. Khanaliloo, M. Mitchell, A. C. Hryciw, and P. E. Barclay. High-Q/V monolithic diamond microdisks fabricated with quasi-isotropic etching. *Nano Lett.* **15**, 5131–5136 (2015).
21. S. Mouradian, N. H. Wan, T. Schröder, and D. Englund. Rectangular photonic crystal nanobeam cavities in bulk diamond. *Appl. Phys. Lett.* **111**, 021103 (2017).
22. Materials and methods are available as supplementary materials on arXiv.
23. J. Lu and J. Vuckovic. Nanophotonic computational design. *Opt. Express* **21**, 13351–13367 (2013).
24. A. Y. Piggott, J. Petykiewicz, L. Su, and J. Vučković. Fabrication-constrained nanophotonic inverse design. *Sci. Rep.* **7**, 1786 (2017).
25. A. Y. Piggott, J. Lu, T. M. Babinec, K. G. Lagoudakis, J. Petykiewicz, and J. Vučković. Inverse design and implementation of a wavelength demultiplexing grating coupler. *Sci. Rep.* **4**, 7210 (2014).

26. F. Van Laere, G. Roelkens, M. Azre, D. Taillaert, D. Van Thourhout, T. F. Krauss, and R. Baets. Compact and highly efficient grating couplers between optical fiber and nanophotonic waveguides. *J. Light. Technol.* **25**, 151–156 (2007).

27. D. Vermeulen, S. Selvaraja, P. Verheyen, G. Lepage, W. Bogaerts, P. Absil, D. Van Thourhout, and G. Roelkens. High-efficiency fiber-to-chip grating couplers realized using an advanced cmos-compatible silicon-on-insulator platform. *Opt. Express* **18**, 18278–18283 (2010).

28. P. Rath, S. Khasminskaya, C. Nebel, C. Wild, and W. H. Pernice. Grating-assisted coupling to nanophotonic circuits in microcrystalline diamond thin films. *J. Light. Technol.* **4**, 300–305 (2013).

29. A. Faraon, C. Santori, Z. Huang, K. M. C. Fu, V. M. Acosta, D. Fattal, and R. G. Beausoleil. Quantum photonic devices in single-crystal diamond. *New J. Phys* **15**, pages = 025010, (2013).

30. A. H. Piracha, P. Rath, K. Ganesan, S. Khn, W. H. P. Pernice, and S. Prawer. Scalable fabrication of integrated nanophotonic circuits on arrays of thin single crystal diamond membrane windows. *Nano Lett.* **16**, 3341–3347 (2016).

31. X. Zhou, I. Kulkova, T. Lund-Hansen, S. Lindskov Hansen, P. Lodahl, and L. Midolo. High-Efficiency Shallow-Etched Grating on GaAs Membranes for Quantum Photonic Applications. <http://arxiv.org/abs/1809.03189> (2018).

32. M. J. Burek, Y. Chu, M. S. Z. Liddy, P. Patel, J. Rochman, S. Meesala, W. Hong, Q. Quan, M. D. Lukin, and M. Lonar. High quality-factor optical nanocavities in bulk single-crystal diamond. *Nat. Comm.* **5**, 5718 (2014).

33. M. Gould, E. R. Schmidgall, S. Dadgostar, F. Hatami, and K.-M. C. Fu. Efficient extraction of zero-phonon-line photons from single nitrogen-vacancy centers in an integrated gap-on-diamond platform. *Phys. Rev. Applied* **6**, 011001 (2016).

34. A. Faraon, I. Fushman, D. Englund, N. Stoltz, P. Petroff, and Vučković.

35. M. J. Burek, C. Meuwly, R. E. Evans, M. K. Bhaskar, A. Sipahigil, S. Meesala, B. Machielse, D. D. Sukachev, C. T. Nguyen, J. L. Pacheco, E. Bielejec, M. D. Lukin, and M. Lončar. Fiber-coupled diamond quantum nanophotonic interface. *Phys. Rev. Applied* **8**, pages = 024026, year = (2017),.

36. J. L. Zhang, S. Sun, M. J. Burek, C. Dory, Y. K. Tzeng, K. A. Fischer, Y. Kelaita, K. G. Lagoudakis, M. Radulaski, Z. X. Shen, N. A. Melosh, S. Chu, M. Lončar, and J. Vučković. Strongly cavity-enhanced spontaneous emission from silicon-vacancy centers in diamond. *Nano Lett.* **18**, 1360–1365 (2018).

37. J. L. O’Brien, A. Furusawa, and J. Vučković. Photonic quantum technologies. *Nat. Photonics* **3**, 687–695 (2009).

38. W. F. Koehl, B. B. Buckley, F. J. Heremans, G. Calusine, and D. D. Awschalom. Room temperature coherent control of defect spin qubits in silicon carbide. *Nature* **479**, 84–87 (2011).

39. T. Zhong, J. M. Kindem, J. G. Bartholomew, J. Rochman, I. Craiciu, E. Miyazono, M. Bettinelli, E. Cavalli, V. Verma, S. W. Nam, F. Marsili, M. D. Shaw, A. D. Beyer, and A. Faraon. Nanophotonic rare-earth quantum memory with optically controlled retrieval. *Science* **357**, 1392–1395 (2017).